Doping-controlled phase transitions in single-layer MoS_{2}

Houlong L. Zhuang, Michelle D. Johannes, Arunima K. Singh, and Richard G. Hennig

Doping-Controlled Phase Transitions in Single-Layer MoS$_2$

Houlong L. Zhuang,[1, 2] Michelle D. Johannes,[3, 1] Arunima K. Singh,[1, 4] and Richard G. Hennig[5, 1, *]

[1]*Department of Materials Science and Engineering,*
Cornell University, Ithaca, New York 14853, U.S.A.
[2]*Department of Mechanical and Aerospace Engineering,*
Princeton University, Princeton, New Jersey 08544, United States
[3]*Naval Research Laboratory, 4555 Overlook Avenue, SW, Washington, DC 20375*
[4]*Joint Center for Artificial Photosynthesis, Lawrence Berkeley National Laboratory, Berkeley, California 94720, U.S.A.*
[5]*Department of Materials Science and Engineering,*
University of Florida, Gainesville, Florida 32611, United States
(Dated: August 8, 2017)

The electronic properties of single-layer MoS$_2$ make it an ideal two-dimensional (2D) material for application in electronic devices. Experiments show that MoS$_2$ can undergo structural phase transitions. Applications of single-layer MoS$_2$ will require firm laboratory control over the phase formation. Here we compare the stability and electronic structure of the three experimentally observed single layer MoS$_2$ phases, $2H$, $1T$, and $1T'$, and an in-plane metal/semiconductor heterostructure. We reveal by density-functional theory calculations that charge doping can induce the phase transition of single-layer MoS$_2$ from the $2H$ to the $1T$ structure. Further, the $1T$ structure undergoes a second phase transition due to the occurrence of a charge-density wave (CDW). By comparing the energies of several possible resulting CDW structures, we find that the $1T'$ orthorhombic structure is the most stable one, consistent with experimental observations and previous theoretical studies. We show that the underlying CDW transition mechanism is not due to Fermi surface nesting, but nonetheless, can be controlled by charge doping. In addition, the stability landscape is highly sensitive to charge doping, which can be used as a practical phase selector. We also provide a prescription for obtaining the $1T'$ structure via growth or deposition of MoS$_2$ on a Hf substrate, which transfers electrons uniformly and with minimal structural distortion. Finally, we show that lateral heterostructures formed by the $2H$ and $1T'$ structures exhibit a low interfacial energy of 0.17 eV/Å, a small Schottky barrier of 0.3 eV for holes and a large barrier of 1.6 eV for electrons.

I. INTRODUCTION

Transition metal dichalcogenides MX$_2$ exhibit a variety of polymorphs due to their unique layered structures and weak interlayer van der Waals interactions.[1] When these materials are reduced to two dimensions, the structures of single-layer MX$_2$ appear equally diverse. For instance, single-layer MoS$_2$, an actively investigated member of the MX$_2$ family for next-generation nanoelectronics applications, is frequently observed in experiments to occur in three distinct phases: $2H$, $1T$, and $1T'$ with vastly different electronic properties.[2–4] Most studies focus on the direct band gap semiconducting $2H$ structure shown in Fig. 1(a) where the top and bottom sulfur sublayers are in an eclipsing configuration. A shift of the top or bottom sulfur layer by $1/3(\vec{a}_1 + \vec{a}_2)$, where $\vec{a}_1$ and $\vec{a}_2$ are the in-plane lattice vectors, gives rise to the metallic $1T$ structure shown in Fig. 1(b), which can function as an efficient catalyst for the hydrogen evolution reaction.[5] Recent experimental work has identified, in addition to the $2H$ and $1T$ phases, a third $1T'$ phase, in which an in-plane distortion of the molybdenum ions accompanies the relative shift of sulfur ions as shown in Fig. 1(c).[4]

The observation of multiple single-layer MoS$_2$ phases is something of a mystery, as the $2H$ ground state is calculated to be significantly more stable than the $1T$ phase[6–8] and exhibits a high transition barrier for the sulfur plane shift, required for formation of the $1T$ phase. The reconstructed $1T'$ phase is more stable than $1T$, though
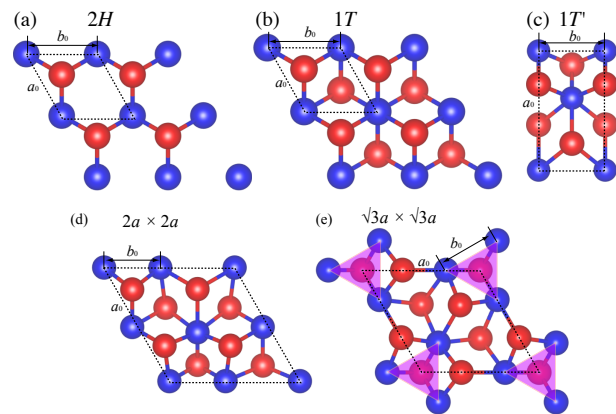

FIG. 1. (Color online) Atomic structures of the (a) $2H$, (b) $1T$, (c) $1T'$, (d) $2a \times 2a$, and (e) $\sqrt{3}a \times \sqrt{3}a$ phases of single-layer MoS$_2$. The unit cells are enclosed by dashed lines. Molybdenum and sulfur atoms are represented by blue and red spheres, respectively.

still higher than $2H$, emerges only from the precursor $1T$ metallic state not directly from the $2H$ semiconducting one.[4] Thus, the observed coexistence of all three phases requires two phase transitions and the stabilization of the highly unfavorable metallic state.

In this paper, we employ density-functional theory to analyze the three MoS$_2$ phases, the two phase transitions and the barriers between them, and the system's response

to charge doping. We start from the energetic stability of the $1T$ and $2H$ structures, which determines the thermodynamic driving force of the transition. We then investigate the energy barrier for a displacive transformation between the polymorphs of 2D MoS_2, which assumes that the transformation occurs by a collective motion of the sulfur atoms in either the top or bottom surface. This mechanism is justified by the experimental observation of perfectly coherent interfaces between the polymorphs of MoS_2.[9] We show that charge doping of either n- or p-type reduces the barrier of the $2H$ to $1T$ phase transition, as well as the energy difference between the two structures and demonstrate that doping via the creation of sulfur vacancies effectively stabilizes the $1T$ phase. For the second transition, we compare the stability of several charge-density wave (CDW) structures modulated from $1T$ single-layer MoS_2 and characterize their electronic structures. We confirm that the $1T'$ structure, *i.e.* an orthorhombic structure is the most stable one, consistent with the experimental and theoretical findings.[9,10] The stability of $1T$ vs. $1T'$ is also controllable by charge doping, but n- and p-type schemes operate oppositely, with the former stabilizing the $1T$ and the latter stabilizing the $1T'$ phase. We suggest that heavy doping, on the order of ± 0.5 electrons per formula unit, can be used to select for a desired phase: semiconducting, metallic, or Dirac cone. We also show that electron doping, well within the magnitude needed to stabilize the metallic phase, is possible using a Hf substrate. Large differences in work function between MoS_2 and Hf initiate significant and uniform electron transfer to MoS_2, while the good lattice matching and lack of physical dopant ions minimize structural distortions. Finally, we model an all MoS_2 semiconductor/metal lateral interface and calculate the band offsets for electronic applications. We find that the interface between the $2H$ and $1T'$ phases of MoS_2 has a low interfacial energy of 0.17 eV/Å and a small offset of 0.3 eV between the valence band maximum of $2H$ and the Fermi level of $1T'$.

II.   METHODS

We perform density-functional theory calculations using the projector-augmented wave method as implemented in the plane-wave code Vienna *ab initio* simulation package (VASP).[11–13] For the exchange-correlation functional we employ the Perdew-Burke-Ernzerhof (PBE) approximation.[14] A cutoff energy of 600 eV for the plane wave basis set is used to ensure an accuracy of the energy of 1 meV/atom. The lattice constants and energy differences are consistent with our previous study using a smaller plane-wave cutoff energy of 400 eV.[8]

The k-point sampling uses the Monkhorst-Pack scheme[15] and employs for the $2H$ and $1T$ single-layer MoS_2 structures a $48 \times 48 \times 1$ mesh for the structural relaxations and a $48 \times 48 \times 7$ mesh for the density of states calculations using the tetrahedron method with Blöchl corrections.[16] The k-point meshes used for optimizing the $1T'$, $2a \times 2a$, $\sqrt{3}a \times \sqrt{3}a$, and $2H$ and $1T'$ heterostructure are $32 \times 48 \times 1$, $24 \times 24 \times 1$, $32 \times 32 \times 1$, and $1 \times 18 \times 1$, respectively. The k-point mesh for the calculations of the density of states for the heterostructure is $4 \times 36 \times 1$.

For the single-layer MoS_2 calculations, a periodic repeat length of 18 Å in the direction perpendicular to the MoS_2 sheet ensures that the interactions between the layers are negligible. The in-plane lattice constants and atomic coordinates are optimized with a force tolerance of 0.001 eV/Å. To simulate the charge doping, we modify the number of valence electrons of the system and compensate this with a uniformly charged background.[17–19] Consequently, adding or removing electrons implies n- and p-type doping, respectively. We calculate the phonon spectrum using the PHONOPY program[20] with the interatomic force constants calculated by VASP using the linear response method based on density-functional perturbation theory.[21,22]

We simulate the interaction between the polymorphs of 2D MoS_2 and a Hf(0001) substrate using a slab geometry with eight layers representing the Hf(0001) substrate. The bottom three layers of Hf(0001) are fixed to their bulk positions. A $7 \times 7 \times 1$, $7 \times 7 \times 1$, $4 \times 6 \times 1$, and $4 \times 4 \times 1$ k-point mesh is employed for the $2H$, $1T$, $1T'$ and 2×2 reconstructions adsorbed on Hf(0001), respectively, which results in a convergence of the binding energies within 2 meV/atom.

The hexagonal Hf(0001) surface provides three different sites (hcp, fcc, and top) for the placement of the MoS_2 polymorphs.[23] We relax all the possible high symmetry configurations of MoS_2 in the $2H$, $1T$, $1T'$ and 2×2 structures on Hf(0001). There are six high-symmetry configurations each for the $2H$, $1T$ and $1T'$ structures, simulated with a simulation cell with 11, 11 and 22 atoms, respectively. The 2×2 structure has four high-symmetry configurations on the Hf substrate and is simulated with a cell of 44 atoms. We report the results of the most stable configuration of MoS_2 polymorphs on Hf(0001).

III.   RESULTS

A.   Semiconducting $2H$ to Metallic $1T$ Transition

We first investigate the semiconducting $2H$ to metallic $1T$ transition in terms of structural, energetic and electronic factors. Table I provides the structural parameters and energies of the two phases. Both phases exhibit nearly identical lattice parameters, which facilitates the formation of a coherent interface as observed in experiment.[4] However, the energy difference between the two structures is rather large at 0.28 eV/atom.

In addition to the energy difference, we calculate the energy barrier between the $2H$ and $1T$ structures utilizing the climbing image nudged elastic band method.[24,25]

TABLE I. Structural parameters, formation energies, ΔE, with reference to the $2H$ structure in units of eV/atom, and fundamental band gaps, E_{g}, in units of eV without and with SOC for various 2D structures of single-layer MoS_2.

| Structure	a_0	b_0	ΔE	$E_{\mathrm{g}}^{\mathrm{w/o\ SOC}}$	$E_{\mathrm{g}}^{\mathrm{w/SOC}}$
$2H$	3.18	3.18	0	1.67	1.60
$1T$	3.18	3.18	0.28	0	0
$1T'$	5.72	3.18	0.18	0	0.05
$2a \times 2a$	6.44	2.77	0.21	0.14	0.10
$\sqrt{3}a \times \sqrt{3}a$	5.67	2.83	0.22	0.57	0.57

FIG. 2. (Color online) Energy landscape along the path between the $1T$ and the $2H$ structure as a function of reaction coordinate and charge doping.

Figure 2 shows the energy landscape between the $1T$ and $2H$ structure as a function of the reaction coordinate and charge doping. Here, the reaction coordinate describes the Euclidean distance along the phase transition path connecting the $1T$ and $2H$ structures. We focus on the energy change along that path with reference to the undoped $1T$ structure in spite of its dynamical instability (see below). Without charge doping, we obtain an energy barrier of 0.52 eV/atom for the transition from $2H$ to $1T$ and 0.24 eV/atom for the reverse transition. The latter energy barrier is also comparable to that of 0.33 eV/atom calculated for the same phase transition in single-layer WS_2.[26]

To compare this energy barrier with thermal activation energies, it is important to understand the nature of this transition. The structural similarities between the $2H$ and $1T$ structures indicate that a likely mechanism involves the collective motion of a group of sulfur atoms and a displacive transformation. Dislocation-like mechanisms can reduce the number of S atoms that are collectively displaced to just a few. As a consequence, the energy barrier for the transformation is obtained by multiplying the energy barrier per sulfur atom with the number of sulfur atoms that are collectively displaced in a transformation step, which significantly increases the barrier.[27] Hence, both the forward and backward reaction are unlikely to occur without charge doping, and once the $1T$ structure is formed, it is kinetically unfavorable to transform back into the $2H$ structure.

Figure 2 illustrates that both n- and p-type doping drastically reduce the energy barrier of the transformation. Furthermore, the energy difference between the $2H$ and $1T$ structures decreases as the electron count for either type of charge doping. Therefore, charge doping may be used to induce the phase transition from the $2H$ to the $1T$ structure. This effect is similar to the proposed charge-transfer mechanism contributing to the $2H$ to $1T$ phase transition in MoS_2 nanotubes.[28] However, our finding provides a more general mechanism of phase transition that may also apply to other single-layer materials such as WS_2.

In practice, the change of the number of electrons can be realized by several commonly used strategies such as
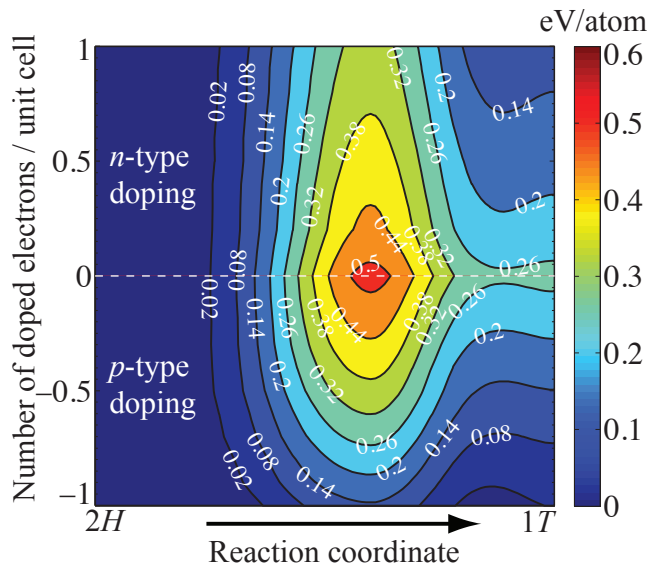
lithium intercalation,[5] incorporation of sulfur vacancies for the p-type doping, chemical functionalization with various functional groups[29] and, as we suggest in this work, charge transfer to or from a substrate. Experimentally, a transmission electron microscope under high electron beam doses could introduce sulfur vacancies into single-layer MoS_2 to induce the phase transformation.[30] A similar experimental technique has been recently used to control the size of $1T$ nanoribbons.[9]

B. Dynamic Instability of Metallic $1T$ MoS_2

We proceed to determine the dynamical stability of the $2H$ and $1T$ phases by calculating their phonon spectra. Figure 3(a) shows that the phonon spectrum of $2H$ single-layer MoS_2 exhibits no imaginary frequencies, confirming the dynamical stability of $2H$ MoS_2, consistent with Ref. 6. By contrast, the phonon spectrum of $1T$ single-layer MoS_2 in Fig. 3(b) displays imaginary frequencies corresponding to dynamically unstable phonon modes. Two acoustic phonon branches of $1T$ MoS_2 are unstable throughout a significant portion of the spectrum, with the strongest softening near the M point.

The imaginary phonon mode at the M point implies a commensurate reconstructed structure. However, the dynamical instability in the second unstable acoustic branch disturbs this simplicity. In other words, the many wavevectors at which the phonon modes become imaginary yield few clues as to the final stable reconstruction. Therefore, we test three CDW structures that are known to occur in three-dimensional MoS_2, $i.e.$ the $1T'$,[31] $2a \times 2a$,[32] and $\sqrt{3}a \times \sqrt{3}a$ reconstructions.[33,34] Note, that the $1T'$ structure is also sometimes called $2a \times a$.[6,7]
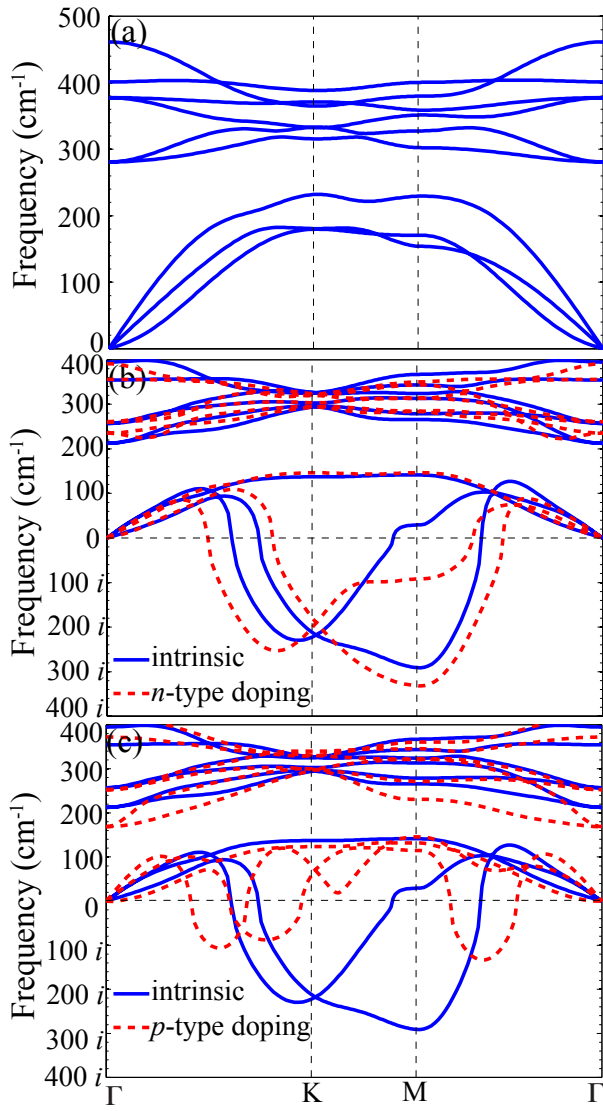
FIG. 3. (Color online) Phonon spectra of (a) $2H$ MoS_2, (b) n-type , (c) p-type doped $1T$ MoS_2. The phonon spectrum of intrinsic $1T$ MoS_2 is shown in both panels (b) and (c) for comparison.

Figure 1 shows the $2H$ and $1T$ structures of MoS_2 as well as various possible reconstructions after geometry optimizations. In the $1T'$ reconstruction, shown in Fig. 1(c), the Mo atom in the middle of the unit cell is displaced upwards along the a_0 axis from its central position. Similarly, in the $2a \times 2a$ reconstruction in Fig. 1(d), the middle column of Mo atoms is displaced leftwards along the b_0 direction, resulting in a shorter interatomic distance with the left column of Mo atoms. The $\sqrt{3}a \times \sqrt{3}a$ reconstruction shown in Fig. 1(e) features the formation of a Mo trimer. Symmetry analysis shows that the $1T'$ structure has space group $P2_1/m$ (11), whereas both the $2a \times 2a$ and $\sqrt{3}a \times \sqrt{3}a$ structures exhibit space groups $P31m$ (157).[35] Table I provides the structural parameters of these reconstructions, denoted
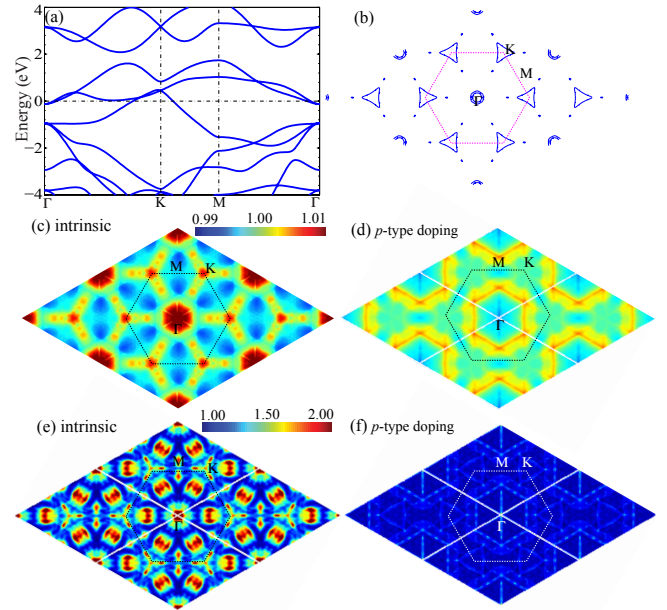

FIG. 4. (Color online) Electronic structure of $1T$ single-layer MoS_2: (a) band structure and (b) Fermi surface, (c) and (d) real part, (e) and (f) imaginary part of the electronic susceptibility, for intrinsic and p-type doped $1T$ MoS_2, respectively.

as a_0 and b_0 in Fig. 1.

The phonon spectra of intrinsic $1T$ single-layer MoS_2 changes with both hole and electron doping, but in an asymmetric manner. For n-type doping with 0.5 electrons per unit cell, the phonon spectrum displayed in Fig. 3(b) shows visible, but minor differences from the intrinsic phonon spectrum and the instability toward $1T'$ remains. In contrast, the p-doped phonon spectrum shown in Fig. 3(c) illustrates a drastic reduction in the magnitude of unstable phonon frequencies. Thus, p-type doping is not only more effective in reducing the energy barrier for the transition from the $2H$ to the $1T$ structure (see Fig. 2) but also acts against the subsequent transition to the $1T'$ phase by reducing the phonon softening.

Table I also compares the formation energies of the $1T'$, $2a \times 2a$, and $\sqrt{3}a \times \sqrt{3}a$ structures with reference to the $2H$ structure. The similarity in energies of these three distorted $1T$ structures may explain why all these structures are experimentally observed in bulk MoS_2.[31–34] The $1T'$ structure displays the lowest energy, consistent with the experimental observation in single-layer MoS_2.[4] A similar CDW structure has also been discovered in single-layer WS_2.[26]

C. Charge-Density Wave for $1T'$ MoS_2

We next characterize the electronic structure of $1T$ MoS_2 to determine if the structural instability has an electronic origin. Figure 4(a) displays the band structure of single-layer MoS_2 within the $1T$ structure. Three bands cross the Fermi level, confirming that $1T$ MoS_2
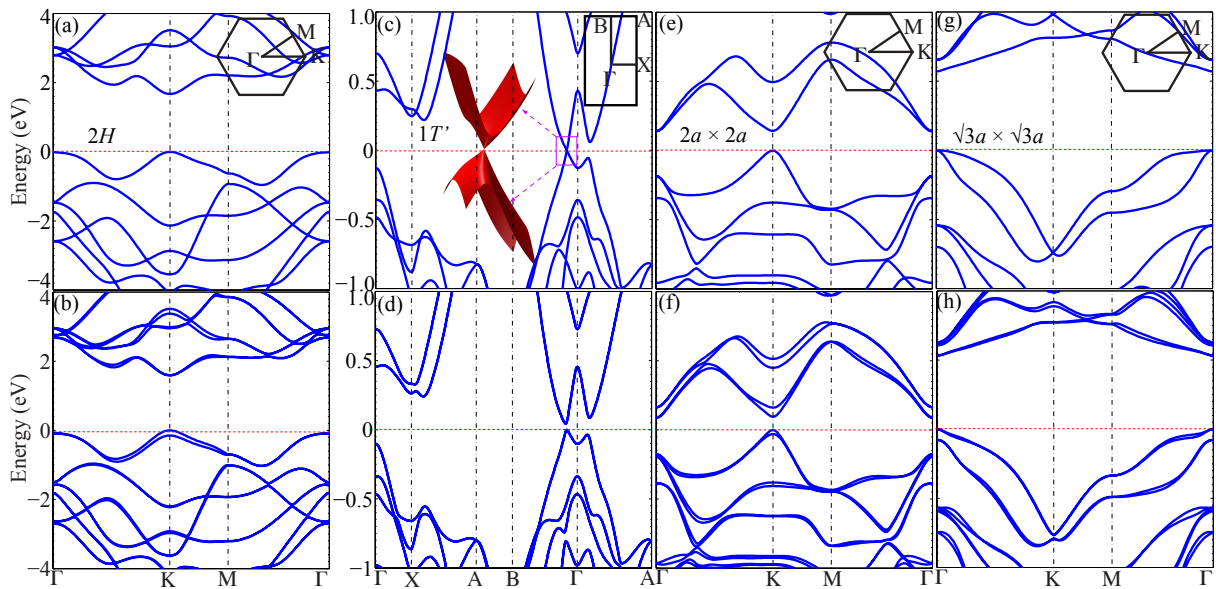
FIG. 5. (Color online) Electronic band structures of the various polymorphs of single-layer MoS_2 exhibiting the (a) $2H$, (c) $1T'$, (e) $2a \times 2a$, and (g) $\sqrt{3}a \times \sqrt{3}a$ structures. The corresponding band structures with SOC are shown in panels (b), (d), (f), and (g). The valence band maximum is set to zero.

exhibits metallic behavior. Figure 4(b) shows that the Fermi surface of $1T$ single-layer MoS_2 is anisotropic and consists of four pockets: (i) two concentric electron pockets near the Γ point, (ii) an elliptic electron pocket along the direction from the Γ to the K point, and (iii) a triangular hole pocket around the K point.

Interestingly, the surfaces of the hole pockets around neighboring K points are almost parallel to each other, giving rise to a significant nesting, which is defined as the superposition of Fermi surfaces when translated one to another by a nesting vector $\mathbf{q}$.[36,37] Fermi surface nesting is often cited as a determining factor in the stability/instability of metallic transition-metal dichalcogenides,[38] towards CDW formation, though we argue here that this is not the case for single-layer MoS_2.

As suggested in previous works on CDW formation, the Fermi surface is only a small part of the energy range from which weight in the susceptibility is gathered.[36,39] We therefore calculate the electronic susceptibility, $\chi(\mathbf{q})$, in the constant matrix element approximation[37] as a real part $\chi'(\mathbf{q})$, which draws from the full energy range and is relevant for CDW formation and as an imaginary part, $\chi''(\mathbf{q})$, which directly reflects the Fermi surface nesting. These two quantities can in both principle and practice have peaks at widely varying wave vectors. The susceptibility, $\chi'(\mathbf{q})$ is given by

$$\chi'(\mathbf{q}) = \sum_{\mathbf{k}} \frac{f(\varepsilon_{\mathbf{k}}) - f(\varepsilon_{\mathbf{k+q}})}{\varepsilon_{\mathbf{k}} - \varepsilon_{\mathbf{k+q}}}, \qquad (1)$$

where $\varepsilon_{\mathbf{k}}$ and $\varepsilon_{\mathbf{k+q}}$ are band energies at the wave vectors $\mathbf{k}$ and $\mathbf{k+q}$, respectively and the numerator is the difference between Fermi functions, $f(\varepsilon)$ at those energies. The nesting function, which is the imaginary part

of the electric susceptibility at $\omega=0$, $\chi''(\mathbf{q})$, is calculated according to the following equation,[39]

$$\lim_{\omega \to 0} \chi''(\mathbf{q}, \omega)/\omega = \sum_{\mathbf{k}} \delta(\varepsilon_{\mathbf{k}} - \varepsilon_F)\delta(\varepsilon_{\mathbf{k+q}} - \varepsilon_F), \qquad (2)$$

where ε_F is the Fermi energy.

Figure 4(c) shows the real part of the electronic susceptibility, $\chi'(\mathbf{q})$, for $1T$ MoS_2, calculated using a dense $100 \times 100 \times 1$ k-point mesh. In the case of MoS_2, the strongest peaks in the nesting function occurs at the K point of the Brillouin zone, with weaker points along the Γ-K direction, but with no visible peak at the M point. The nesting peaks do carry over into $\chi'(\mathbf{q})$, but their separation from the CDW wave vector eliminates Fermi surface nesting as the driving force of the transition to the $1T'$ structure.

The electronic structure could, however, still be an important ingredient, entering through the electron-phonon coupling that softens the phonons. For instance, the nesting function enters directly into the electron-phonon coupling constant, λ,[39] relevant to superconductivity, and the phonon renormalization (softening) that can result in imaginary frequencies is proportional to $\chi'(\mathbf{q})$. The prevalent softening of the phonons around the K point seen in the spectrum of Fig. 4(c) may, therefore, stem from structure in $\chi'(\mathbf{q})$. However, the equal or stronger softening elsewhere that gives rise to the $1T'$ structure cannot be related to the electronic susceptibility $\chi(\mathbf{q})$ and is more likely the result of strengthened electron-phonon matrix elements, as has been experimentally and theoretically observed in other materials.[40]

Next, we investigate how charge doping affects the nesting, i.e. the imaginary part of the electronic susceptibility. As discussed above, n-type doping only weakly

affects the phonon modes of $1T$ MoS$_2$. We observe that the Fermi surface nesting is almost unaffected by n-type doping. In contrast, p-type doping significantly decreases the $\chi'(\mathbf{q})$ peaks and the corresponding nesting peaks in $\chi''(\mathbf{q})$, as seen in Figs. 4(d) and (f), respectively, which furthermore acts toward stabilization of phonons across the entire spectrum. This again supports our suggestion that p-type doping is a more effective strategy to stabilize the $1T$ structure.

D. Electronic structure of the MoS$_2$ Polymorphs

Figure 5 displays the electronic band structures of $2H$ single-layer MoS$_2$ and the various reconstructions of the $1T$ structure. Figure 5(a) shows that $2H$ MoS$_2$ exhibits a PBE band gap of 1.67 eV, consistent with previous calculations and slightly smaller than the experimental optical band gap of 1.90 eV.[41,42] Figure 5(c) shows the electronic band structure of the $1T'$ structure, identified as the lowest energy reconstruction. Interestingly, a Dirac cone is formed between the B and Γ points as illustrated in the inset in Fig. 5(c).[10] Figures 5(e) and (g) depict the electronic band structures of the $2a \times 2a$ and $\sqrt{3}a \times \sqrt{3}a$ phases, respectively. In contrast to the $1T'$ structure, these two structures are semiconducting with direct band gaps of 0.14 and 0.57 eV as summarized in Tab. I.

Spin-orbit coupling (SOC) is known to affect the electronic structures of single-layer transition-metal dichalcogenides,[43] and we determine how it changes the electronic band structure of all of the five single-layer MoS$_2$ polymorphs. For $2H$ MoS$_2$, shown in Fig. 4(b), the SOC results in a splitting of the valence band maximum of at the K point by 0.149 eV, which agrees with a previously reported value of 0.146 eV.[43] For the $1T'$ structure, the SOC splits the Dirac cone, opening a band gap of 50 meV, as seen in Fig. 4(d). This band gap agrees well with a recently reported value of around 80 meV.[10] The band gap opening due to SOC is of particular interest, as it is related to 2D topological insulators.[10,44] SOC also decreases the band gap of the $2a \times 2a$ structure, while the band gap of the $\sqrt{3}a \times \sqrt{3}a$ structure is almost unaffected by the SOC.

E. Substrate Stabilization of MoS$_2$ Polymorphs

Our study shows that charge doping can be used to stabilize one polymorph of single-layer MoS$_2$ over another. However, changing the charge via sub- or super-valent dopants on the level of ± 0.5 electrons per formula unit will likely cause significant structural distortions in the host crystal structure of MoS$_2$ or could even exceed the solubility limit for the dopant, resulting in the formation of competing phases, thus decreasing or eliminating the possibility of dopant induced polymorph stabilization. As shown in our previous work on the synthesis of 2D group III-V materials on metal substrates, a dif-
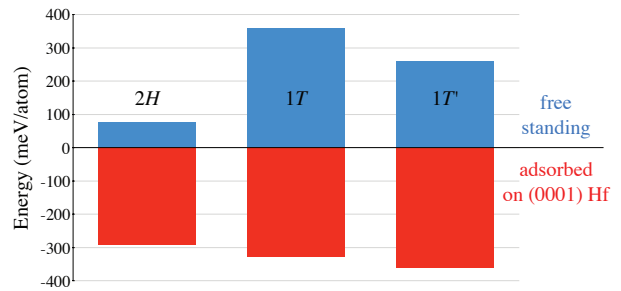

FIG. 6. (Color online) Formation energy relative to the 3D bulk phase of MoS$_2$ for the three single-layer polymorphs of MoS$_2$ when free standing and adsorbed on a Hf(0001) substrate. Adsorption on Hf(0001) leads to electron doping and stabilizes the $1T'$ polymorph.

ference in the work function of the substrate and a 2D material can lead to charge doping.[23] Similar observations have been made for graphene adsorbed on transition metal substrates.[45] We suggest that adsorption of single-layer MoS$_2$ on suitable substrates can provide pure charge doping and hence be used to control the structure of MoS$_2$.

To stabilize or synthesize the polymorphs of MoS$_2$, we search for symmetry matched substrates with small lattice mismatch, which should minimize strain induced changes in the electronic properties of the polymorphs as well as dope and stabilize the MoS$_2$ polymorphs. We select the Hf(0001) substrate to provide an example that illustrates our strategy of substrate selection, which can then be used to identify other suitable substrates.

The Hf(0001) surface exhibits a lower work function of 3.9 eV[46] than single-layer MoS$_2$ with a value of 5.1 eV,[8] which should lead to electron doping in the MoS$_2$ polymorphs. Furthermore, Hf(0001) is closely symmetry matched and provides small lattice mismatches for the various MoS$_2$ polymorphs. The lattice parameter of $1T$ and $2H$ MoS$_2$ are smaller than that of the Hf (0001) surface by only 0.4%, while the 2×2 reconstruction of MoS$_2$ has a lattice parameter which is larger by 0.8% compared to the Hf(0001) lattice parameters. One of the $1T'$ MoS$_2$ lattice vectors is larger than the Hf(0001) lattice vector by 3.4%, and the other is smaller by 0.6%. To accommodate the effect of strain, the polymorphs of MoS$_2$ are strained to match the lattice vectors of the Hf(0001) surface.

Figure 6 shows the change in formation energy of the three single-layer phases when adsorbed on a Hf(0001) substrate. The presence of the substrate leads to a charge doping of 0.6 electrons into the $2H$ and $1T$ phases and 0.2 electrons into the $1T'$ phase. The electron doping has a threefold effect on the phase stability of the system. First, the ground state energy of the $1T$/substrate is lower than the $2H$/substrate system. Second, we compute the energy barrier of the transition from $2H$ to $1T$ using the nudged-elastic band method and find that the activation energy barrier is lowered to 0.42 eV/atom in
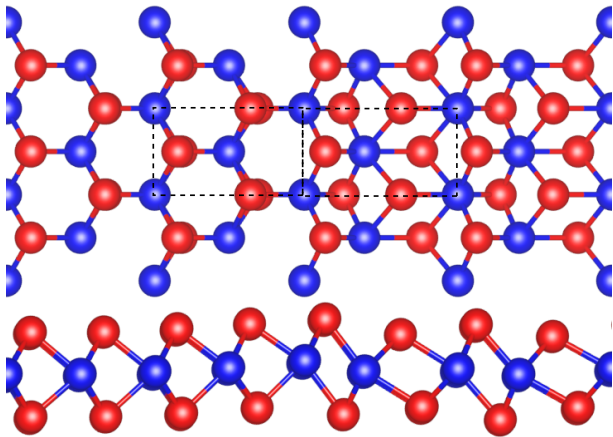
FIG. 7. (Color online) Top and side view of the $2H/1T'$ heterostructure after geometry optimizations. The dashed lines illustrate rectangular unit cells of the $2H$ and $1T'$ structures.

the presence of the substrate, in close alignment with the results of Fig. 2 for the addition of ~ 0.6 electrons. And finally, the electron doping improves the stability of the $1T'$ structure relative to the $1T$ structure. Thus, growth or deposit of MoS_2 onto a Hf substrate is a realistic and achievable route to stabilize the metallic $1T$ polymorph or the small band gap topological insulator $1T'$ polymorph, opening up attractive possibilities for their use as a conductive alternative to graphene in nanoelectronics applications.

F.   Lateral $2H/1T'$ Heterostructure

Finally, we study the effects the occurrence of the $1T'$ structure within $2H$ MoS_2 has on the energetics and the electronic properties. To simulate the interface structure, we construct a supercell of nine rectangular cells of each structure, leading to two interfaces due to the periodic boundary condition. Figure 7 illustrates the interface structure after geometry optimizations with a force tolerance of 0.025 eV/Å. Similar to the definition of the grain boundary energy of single-layer MoS_2,[47] we define the interfacial energy

$$E_{\mathrm{int}} = \frac{E_{2H/1T'} - 1/2(E_{2H} + E_{1T'})}{2l_0},$$

where $E_{2H/1T'}$, E_{2H}, and $E_{1T'}$ are the total energies of the heterostructure, the $2H$ structure, and the $1T'$ structure, respectively, and l_0 is the interface length in the simulation supercell. All energies are calculated using a total of 18 rectangular cells, two of which are illustrated by the dashed lines in Fig. 7. We determine the interfacial energy as 0.17 eV/Å, much smaller than the calculated energies of grain boundaries in $2H$ MoS_2 of at least 0.35 eV/Å.[47] This implies that forming the $2H/1T'$ interface is more favorable than creating different grain boundaries.
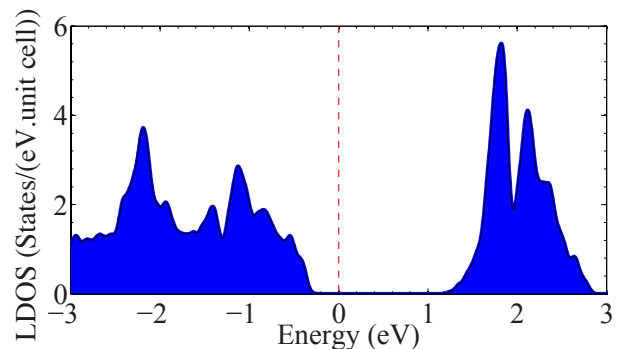

FIG. 8. (Color online) Local electronic density of states of one unit of $2H$ single-layer MoS_2 which is far away from the interface of the $2H/1T'$ heterostructure.

Figure 8 shows the local density of states (LDOS) of a formula unit of $2H$ MoS_2, which is sufficiently far (> 2.5 nm) away from the interface to reduce the effect of the boundary on the electronic structure of pure $2H$ single-layer MoS_2. The offset between the valence band maximum of $2H$ MoS_2 and the Fermi level of $1T'$ MoS_2 extracted from the LDOS is 0.32 eV. Correspondingly, the offset between the conduction band minimum and the Fermi level or Schottky barrier is 1.58 eV, when taking into account the underestimation of the experimental band gap by the PBE functional. The valence and conduction band offsets represent the energy barriers for hole and electron transport, respectively, across the $2H/1T'$ interface. Therefore, we expect that the appearance of the $1T'$ structure decreases the carrier mobility when $2H$ single-layer MoS_2 is used for electronic applications such as nanotransistor.

IV.   CONCLUSIONS

In summary, we studied two types of phase transitions in single-layer MoS_2 and the resulting electronic structure of the different phases. For the phase transition from the $2H$ to $1T$ structure, we find that charge doping of either n or p type lowers the transition barrier and induces the phase transition. We show that charge-doping controls the phase transition from the $1T$ phase to the reconstructed $1T'$ structure, with p-type doping having a larger effect. The simultaneous existence of all three phases, $2H$, $1T$, and $1T'$, despite very high barriers at stoichiometry suggests that intrinsic charge doping may exist and that intentional n- and p-type doping are possible routes towards stabilizing the metallic $1T$ phase against the other two gapped phases. We show that very high charge doping, is needed for this stabilization, but may be achieved uniformly and without significant structural distortion by growth or deposit of single layer MoS_2 on a Hf(0001) substrate. Furthermore, we confirm that the $1T'$ structure has the lowest energy among the four possible polymorphs of $2H$ single-layer MoS_2 in agree-

ment with the experimental observation and previous theoretical prediction. We additionally estimated the energy barriers met by the charge carriers in the $2H/1T'$ heterostructure. Our work opens the realistic possibility of using metallic MoS_2 as an alternative to graphene metallic leads for van der Waals heterostructures.[48]

* rhennig@ufl.edu
[1] J. Wilson and A. Yoffe, Adv. Phys. **18**, 193 (1969).
[2] B. Radisavljevic, A. Radenovic, J. Brivio, V. Giacometti, and A. Kis, Nature Nanotech. **6**, 147 (2011).
[3] D. Jariwala, V. K. Sangwan, L. J. Lauhon, T. J. Marks, and M. C. Hersam, ACS Nano **8**, 1102 (2014).
[4] G. Eda, T. Fujita, H. Yamaguchi, D. Voiry, M. Chen, and M. Chhowalla, ACS Nano **6**, 7311 (2012).
[5] M. A. Lukowski, A. S. Daniel, F. Meng, A. Forticaux, L. Li, and S. Jin, J. Am. Chem. Soc. **135**, 10274 (2013).
[6] M. Calandra, Phys. Rev. B **88**, 245428 (2013).
[7] M. Kan, J. Y. Wang, X. W. Li, S. H. Zhang, Y. W. Li, Y. Kawazoe, Q. Sun, and P. Jena, J. Phys. Chem. C **118**, 1515 (2014).
[8] H. L. Zhuang and R. G. Hennig, J. Phys. Chem. C **117**, 20440 (2013).
[9] Y.-C. Lin, M. O. Dumcenco, Y.-S. Huang, and K. Suenaga, Nature Nanotech. **9**, 391 (2014).
[10] X. Qian, J. Liu, L. Fu, and J. Li, Science **346**, 1344 (2014).
[11] G. Kresse and J. Furthmüller, Phys. Rev. B **54**, 11169 (1996).
[12] P. E. Blöchl, Phys. Rev. B **50**, 17953 (1994).
[13] G. Kresse and D. Joubert, Phys. Rev. B **59**, 1758 (1999).
[14] J. P. Perdew, K. Burke, and M. Ernzerhof, Phys. Rev. Lett. **77**, 3865 (1996).
[15] H. J. Monkhorst and J. D. Pack, Phys. Rev. B **13**, 5188 (1976).
[16] P. E. Blöchl, O. Jepsen, and O. K. Andersen, Phys. Rev. B **49**, 16223 (1994).
[17] C. Si, W. Duan, Z. Liu, and F. Liu, Phys. Rev. Lett. **109**, 226802 (2012).
[18] S. Lany and A. Zunger, Phys. Rev. B **78**, 235104 (2008).
[19] C. Freysoldt, J. Neugebauer, and C. G. Van de Walle, Phys. Rev. Lett. **102**, 016402 (2009).
[20] A. Togo and I. Tanaka, Scr. Mater. **108**, 1 (2015).
[21] S. Baroni, S. de Gironcoli, A. Dal Corso, and P. Giannozzi, Rev. Mod. Phys. **73**, 515 (2001).
[22] M. Gajdoš, K. Hummer, G. Kresse, J. Furthmüller, and F. Bechstedt, Phys. Rev. B **73**, 045112 (2006).
[23] A. K. Singh, H. L. Zhuang, and R. G. Hennig, Phys. Rev. B **89**, 245431 (2014).
[24] G. Mills, H. Jónsson, and G. K. Schenter, Surf. Sci. **324**, 305 (1995).
[25] B. J. Berne, D. F. Coker, and G. Cicotti, *Classical and Quantum Dynamics in Condensed Phase Simulations* (World Scientific Publishing Company, 1998).
[26] D. Voiry, H. Yamaguchi, J. Li, R. Silva, D. C. B. Alves, T. Fujita, M. Chen, T. Asefa, V. B. Shenoy, G. Eda, and M. Chhowalla, Nature Mater. **12**, 850 (2013).
[27] R. G. Hennig, D. R. Trinkle, J. Bouchet, S. G. Srinivasan, R. C. Albers, and J. W. Wilkins, Nature Mater. **4**, 129 (2005).
[28] A. N. Enyashin, L. Yadgarov, L. Houben, I. Popov, M. Weidenbach, R. Tenne, M. Bar-Sadan, and G. Seifert, J. Phys. Chem. C **115**, 24586 (2011).
[29] Q. Tang and D.-e. Jiang, Chem. Mater. **27**, 3743 (2015).
[30] H.-P. Komsa, J. Kotakoski, S. Kurasch, O. Lehtinen, U. Kaiser, and A. V. Krasheninnikov, Phys. Rev. Lett. **109**, 035503 (2012).
[31] J. Heising and M. G. Kanatzidis, J. Am. Chem. Soc. **121**, 638 (1999).
[32] D. Yang, S. J. Sandoval, W. M. R. Divigalpitiya, J. C. Irwin, and R. F. Frindt, Phys. Rev. B **43**, 12053 (1991).
[33] F. Wypych, T. Weber, and R. Prins, Chem. Mater. **10**, 723 (1998).
[34] F. Wypych and R. Schollhorn, J. Chem. Soc. Chem. Commun. , 1386 (1992).
[35] H. T. Stokes and D. M. Hatch, J. Appl. Crystallogr. **38**, 237 (2005).
[36] E. Canadell and M. H. Whangbo, Chem. Rev. **91**, 965 (1991).
[37] M. Calandra and F. Mauri, Phys. Rev. Lett. **106**, 196406 (2011).
[38] M. H. Whangbo and E. Canadell, J. Am. Chem. Soc. **114**, 9587 (1992).
[39] M. D. Johannes and I. I. Mazin, Phys. Rev. B **77**, 165135 (2008).
[40] D. Lamago, M. Hoesch, M. Krisch, R. Heid, K.-P. Bohnen, P. Boni, and D. Reznik, Phys. Rev. B **82**, 195121 (2010).
[41] H. Shi, H. Pan, Y.-W. Zhang, and B. I. Yakobson, Phys. Rev. B **87**, 155304 (2013).
[42] K. F. Mak, C. Lee, J. Hone, J. Shan, and T. F. Heinz, Phys. Rev. Lett. **105**, 136805 (2010).
[43] A. Ramasubramaniam, Phys. Rev. B **86**, 115409 (2012).
[44] Z. F. Wang, Z. Liu, and F. Liu, Nature Commun. **4**, 1471 (2013).
[45] G. Giovannetti, P. A. Khomyakov, G. Brocks, V. M. Karpan, J. van den Brink, and P. J. Kelly, Phys. Rev. Lett. **101**, 026803 (2008).
[46] H. B. Michaelson, J. Appl. Phys. **48**, 4729 (1977).

[47] X. Zou, Y. Liu, and B. I. Yakobson, Nano Lett. **13**, 253 (2013).

[48] A. K. Geim and I. V. Grigorieva, Nature **499**, 419 (2013).